# Augmented design for a fully automated alignment system at the Magdalena Ridge Observatory Interferometer

James J. D. Luis[a], Robert Blasi[b], David F. Buscher[a], Allen Farris[b], Robert Kelly[b], and Robert Ligon[b]

[a]Cavendish Laboratory, University of Cambridge, 19 J J Thompson Avenue, Cambridge, CB3 0HE, UK

[b]Magdalena Ridge Observatory, New Mexico Institute of Mining and Technology, 801 Leroy Place, Socorro, NM, 87801

## ABSTRACT

Stable beam alignment of an optical interferometer is crucial for maintaining a usable signal-to-noise ratio during science measurements on faint astronomical targets. The Magdalena Ridge Observatory Interferometer will use an Automated Alignment System (AAS) that performs a start-of-night alignment procedure and subsequent alignment corrections in between observations, all without the need for human intervention. Its design has recently been updated in line with a revised error budget for MROI requiring that two axis drifts during science operations should not exceed 15 milliarcseconds in tilt, referred to the sky, nor 1% of the beam diameter in shear. For each beam line, the AAS provides two reference light beams, a pair of quad cells to monitor coarse alignment, and a tilt and shear detector for tracking fine drifts. The tilt and shear detector is a novel application of a Shack-Hartmann array that permits the simultaneous measurement tilt and shear well within requirements for MROI. Results of laboratory testing and simulations are presented here.

**Keywords:** automated alignment, Shack-Hartmann, Magdalena Ridge Observatory Interferometer

## 1. INTRODUCTION

Optical amplitude interferometers combine beams of starlight to produce fringes. The fringe contrast and phase depends not only on the angular brightness distribution of the source but also on the relative alignment of the beams. To maximise visibility, the beams should be perfectly overlapped at the detection plane with a known tilt between them. Beams that drift in tilt (angular direction) and shear (transverse position) therefore result in a reduced signal-to-noise ratio for science measurements. Stable beam alignment will therefore be crucial for meeting the sensitivity goal of the Magdalena Ridge Observatory Interferometer (MROI).[1] We are designing an Automated Alignment System (AAS) for MROI that will not only align the unit telescope beam trains at the beginning of the night but will also periodcally correct for drifts during the night. An error budget for MROI has been allocated such that for a single beam arriving at the science detector after start-of-night beam train alignment, the uncertainty in tilt is no more than 15 milliarcseconds, referred to the sky, and uncertainty in shear is no more than 1% of the beam diameter. Subsequent drifts in tilt and shear are similarly not allowed to exceed 15 milliarcseconds on sky or 1% of the beam diameter, respectively. The initial alignment of all ten

Further author information: (Send correspondence to J. J. D. Luis)
E-mail: jjdl3@mrao.cam.ac.uk, Telephone: +44 1223 337 137

telescope beam trains must take no longer than one hour, while the intra-night corrections should be diagnosed and applied within one minute per five-minute science observation. Sampling of the alignment must not reduce throughput to the science beam combiner by more than 3%.

The previous design for the AAS proposed by Shtromberg et al.[2] has been updated following a revision of the overall error budget for MROI. In particular the following aspects have been modified:

- The AAS now includes a tilt and shear detector in each of the unit telescope beam trains - this was previously a distinct subsystem of the interferometer known as Back End Active Stabilisation of Shear and Tilt (BEASST).
- A single light source marked the optical axis in the absence of bright starlight, but could only be injected by means of a flip-in beam splitter. The new design contains light sources at two locations in each telescope beam train, allowing intra-night alignment to be checked at any time by simply switching on a light source at each unit telescope.
- The large aperture quad cells at two mirrors in the beam relay are now double-sided to permit detection of light propagating in both directions along the beam train.
- The splitting of the light source in the Beam Combining Area between the ten beam lines was hoped to be achieved with broadband fibre splitters. Unfortunately this scheme did not meet requirements in practice, so we have instead devised a method of free-space distribution.

The requirements for this version of the AAS are demanding so we constructed laboratory prototypes of the key components to mitigate technical risk ahead of its deployment at MROI.

## 2. CONCEPTUAL DESIGN

### 2.1 Beam train optics

The path of light from one unit telescope (UT) to the beam combining instruments is summarised in Figure 1. We define the optical axis using artificial light sources in two locations. One is in the Beam Combining Area (BCA) and has come to be known as the Magic Optical Box (MOB); the other is at the Nasmyth table of the UT and is known as UTLIS. The alignment of the beams is sampled by a collection of detectors:

- A large photovoltaic quad cell at mirrors M4 and M5 in the relay for every beam train. Each quad cell can be flipped into the beam when needed.
- A tilt and shear detector for each beam train in the BCA, close to the beam combiners, known as BEASST.
- An electron multiplying CCD camera owned by the fast tip-tilt correction system.[3]
- A tilt and shear detector for each of the fringe tracker, visible science combiner and infrared science combiner, able to view one beam at a time.

### 2.2 Start of night alignment

Start-of-night alignment commences prior to astronomical twilight. The following general steps are followed:

1. Align the MOB beam with the delay line axis, diagnosed by the quad cell at mirror M5 in the beam relay.
2. Switch on UTLIS so that the tilt and shear of the UTLIS and MOB beams can be measured by BEASST
3. Tweak tip-tilt of mirrors M4 and M5 to overlap the UTLIS fiducials with the MOB fiducials at BEASST.
4. Set the fiducial of the fast tip-tilt correction system as the centroid of the spot produced by UTLIS. Thereafter, starlight captured with the telescope is aligned in tilt with the UTLIS beam.

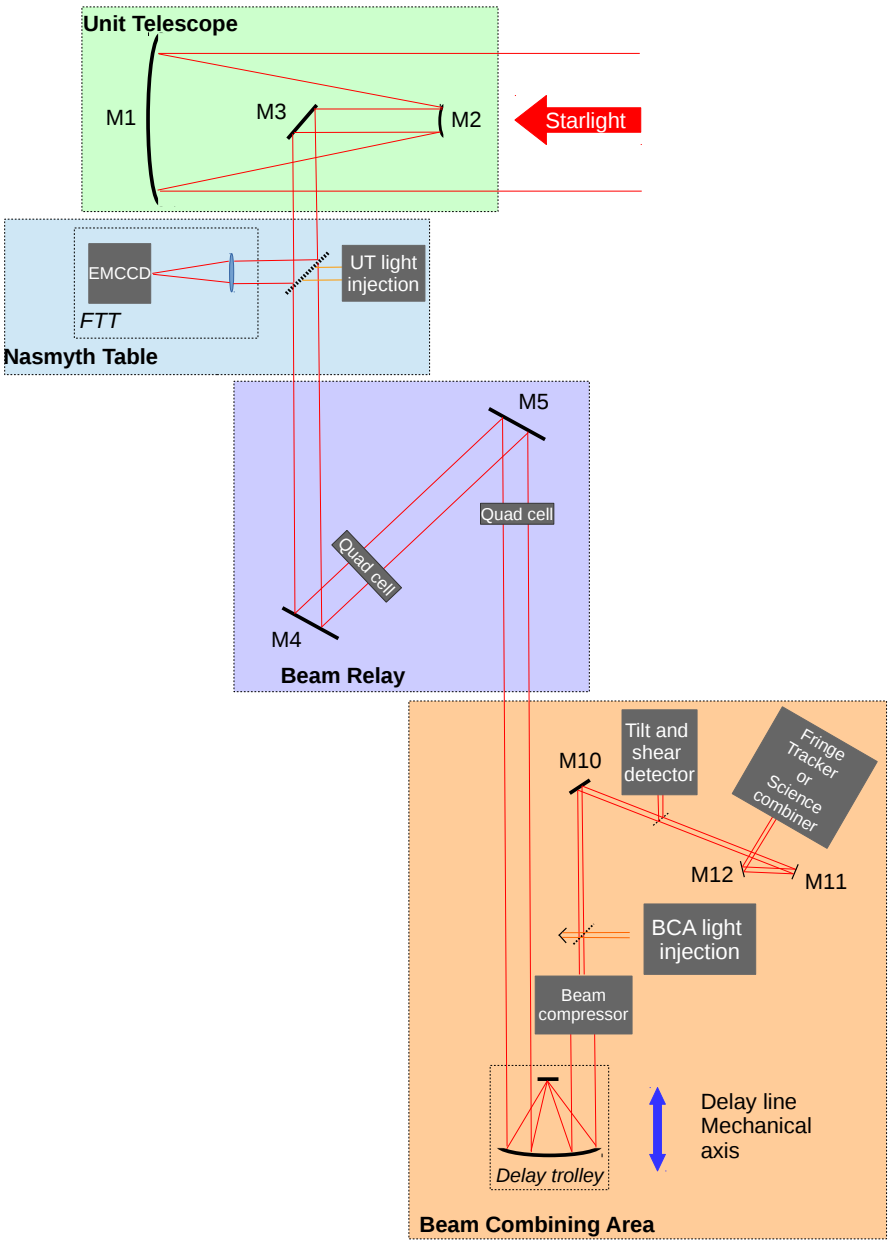


Figure 1: Single beam line from a unit telescope of MROI through to the beam combiners. The optical components are distributed among the Unit Telescope, Nasmyth Table, Beam Relay and Beam Combining Area.

5. Record residual shear between starlight and UTLIS with BEASST as an offset for later measurements.
6. Using MOB as a proxy for starlight, use mirrors M11 and M12 to steer beams into the fringe tracker and science combiners
7. Internally align fringe tracker and science combiners, borrowing light from the MOB.

### 2.3 Intra-night alignment

The alignment of the beam train will be queried by BEASST in between science observations using either bright starlight or UTLIS if the star under observation is too dim. A pair of mirrors is tasked with counteracting drifts in both tilt and shear. Mirrors M4 and M5 are prime candidates for this job, partly because they are exposed to outdoor temperatures and so are likely to themselves be the cause of alignment drifts. The relative alignment between the UTLIS and starlight will of course be likely to drift too. This can be partially corrected whenever the UT light source is switched on, since the fiducial on the FTT camera can be reset to its shifted centroid. This does however leave a relative shear between the alignment and starlight beams. This shear can only be determined when observing bright starlight on the tilt and shear detector in the BCA, at which point the offset can be recorded and the BCA alignment beam be overlapped with starlight. We must therefore slew the UT to a bright star from time to time in order to check this.

## 3. KEY HARDWARE COMPONENTS

In this section, we describe the key components of the AAS in more detail. Results of the current state of prototyping are also reported here.

### 3.1 Unit telescope light injection

The wavelengths of the light source are 808nm and 1550nm. We choose 808nm to be detected within the sensitive range of the FTT electron multiplying CCD camera and on the photovoltaic panels of the quad cells. The 1550nm light is primarily for BEASST, but may also serve the alignment camera of the infrared science combiner. The light will originate in an electronics cabinet in the enclosure for the UT. The two wavelengths are generated by laser diodes and combined by a plate splitter before being coupled into an endlessly single-mode photonic crystal fibre. We may run these lasers below threshold to reduce heat dissipation in the cabinet and to reduce the temporal coherence of the beam so that fringes do not form from parallel window reflections.

The fibre is routed to the Nasmyth table adjacent to the telescope. Light emerging from the end of the fibre is collimated by a custom cemented doublet of SF5 and N-SF6 glasses that offers achromatic performance at 808nm and 1550nm. Although the starlight beam relay diameter is 95mm, the diameter of UTLIS is chosen to be 50mm in order to match the size of the sensitive region of the quad cells. Nevertheless the Rayleigh distances at 808nm and 1550nm are 2.4km and 1.3km respectively, which are both several times greater than the maximum beam path of MROI. The alignment source is coupled into the UT beam train using the dichroic mirror that samples starlight for fast tip-tilt correction, therefore injection of this light source does not cause any loss to starlight throughput. Alignment is achieved by two flat mirrors held in steerable mounts. Figure 2 displays how the collimating and steering optics will fit within a space envelope on the Nasmyth Table.

We tested the effect of temperature drifts on a commercially available 3-inch diameter mirror mount possessing only two tip-tilt actuators. It turns out that the pivoting caused by differential expansion provoked a tilt that exceeded the seasonal drift allowance by several times. A more favourable design uses three identical motorised actuators on each mount, thereby almost entirely eliminating this tilt drift.

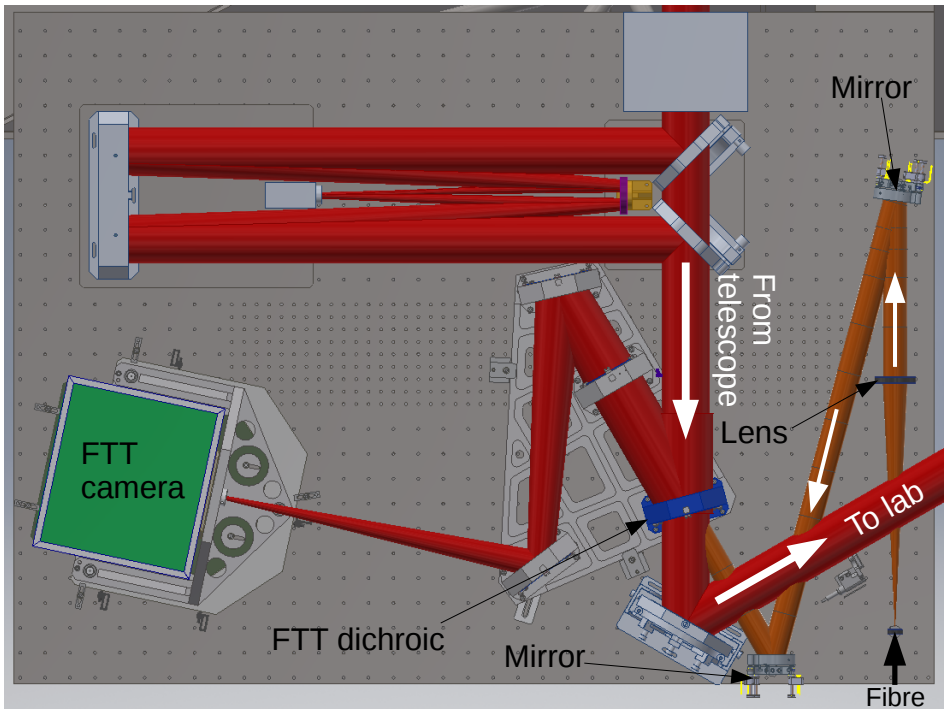


Figure 2: Birdseye view of the UT light source injection into the beam line on the Nasmyth Table. The UTLIS is colored in orange while the starlight beam is red. Starlight arrives from the top and is directed to the right. The blue optical mount is the FTT dichroic splitter through which UTLIS is injected into the telescope beam train.

## 3.2 Beam combining area light injection

### 3.2.1 Design

The MOB distributes light from a common broadband source to each of the ten beam lines. Light is injected both upstream to the UTs and downstream to the fringe tracker and science combiners. Each beam marks the optical axis to align the optics from the BCA through to the UT enclosures. In the opposing direction, the light enables the fringe tracker and science combiners to be aligned. Additionally, piston can be measured, both for the constant delay term of each beam train and for path differences between the fringe tracker and science combiner, since the light for all beam lines originates from the same incoherent source.

Our proposed design comprises of four parts:

1. Light generation and coupling from two sources
2. Beam splitting and distribution
3. Optical path length compensation
4. Injection into telescope beam trains

The light source is a combination of a tungsten-halogen lamp and a visible laser diode. Heat dissipation in the inner BCA must be minimised to avoid provoking laboratory seeing. Hence the lamp was selected from a low-power flashlight and the laser light is distributed to the optical table via a single-mode fibre, with the diode itself concealed in an electronics cabinet in an outer area of the building. The filament of the lamp is 35$\mu$m in

diameter and draws less than 1W of electrical power. It will be switched off during science observations. The laser and white light are collimated by achromatic doublets and combined by a 90:10 cube splitter. The beam is then focussed on a pinhole using another achromatic doublet. The pinhole is smaller than the diameter of the imaged filament. Light diverges from the pinhole and is collimated by a silver-coated off-axis parabola to ensure achromatism across the spectral range. The beam is truncated to the compressed beam diameter of the starlight beam (ie 13mm) before being steered onwards by two plane mirrors. These mirrors align the beam to an arrangement of beam splitters that divide the beam amongst the ten telescopes.

An initial beam distribution scheme is depicted in Figure 3. We have chosen an eight-way division of beams by cube splitters. Each output beam will have experienced three splits. Unlike for plate splitters, this allows each of the output beams to traverse the same amount of dispersive material in order to minimise group delay differences between beams.[4] To serve the full set of ten beam trains, an additional splitter and dispersion compensator must be installed. Off-the-shelf antireflection coatings are not sufficiently broadband to cover all of the R, I, J, H and K bands. We may design a custom multilayer coating based on the work of Hobson and Baldwin,[5] which demonstrated a viable solution with under 1% reflection for wavelengths from 0.6$\mu$m to 2.4$\mu$m.

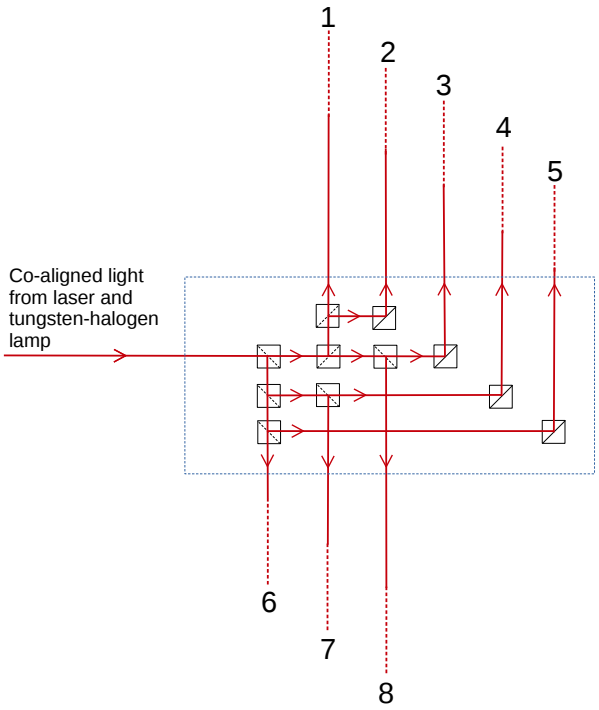


Figure 3: Scheme to divide an input light beam eight ways using cube splitters.

Next, each beam encounters a vertically-aligned roof mirror to reflect the beam back parallel to the incoming beam but offset in the vertical direction. This optic is mounted on a linear translation stage with minimum incremental motion of 0.1$\mu$m with which to equalise optical path differences between output beams.

The final stage is injection into the beam trains. We achieve two-way coupling with a 50:50 cube splitter and a corner cube. The latter is mounted on a two-axis linear translation stage to remove any shear between the transmitted and reflected beams. The splitter is mounted on a translation stage for injection on demand so that starlight throughput is not reduced during science measurements. A birdseye view of the table housing the optics is shown in Figure 4.

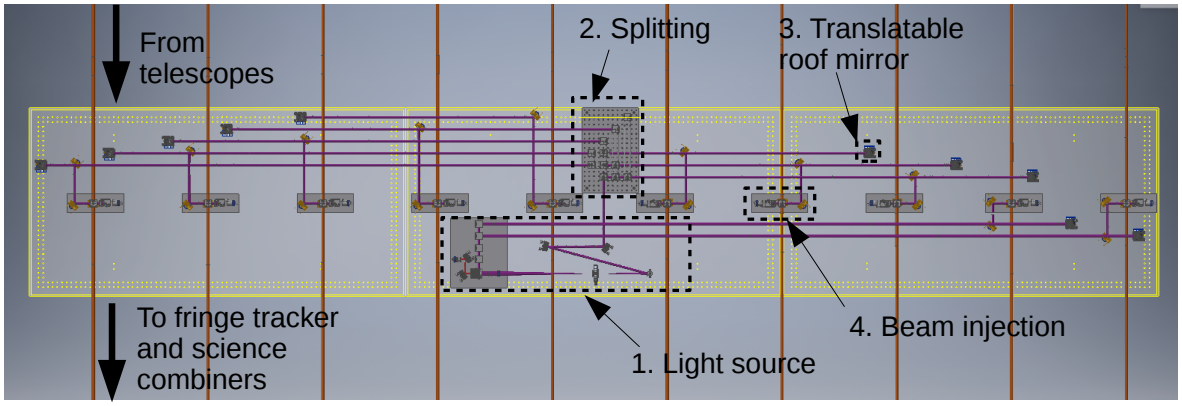


Figure 4: Birdseye view of BCA light source injection into beam trains. The alignment beams are shown in purple while the starlight beams for the ten beam trains are shown in orange. All beams are nominally 13mm in diameter in this section of the beam train. Light is generated in the centre of the table, then distributed amongst the 10 beams. A delay is applied for each beam in the left-right direction of this figure.

### 3.2.2 Laboratory prototyping

We have built the eight-way splitting scheme and the translatable roof mirror, as photographed in Figures 5 and 6. Initial tests have been conducted at visible wavelengths. Figure 7 shows a pupil plane interference pattern between two outputs of the distribution optics.

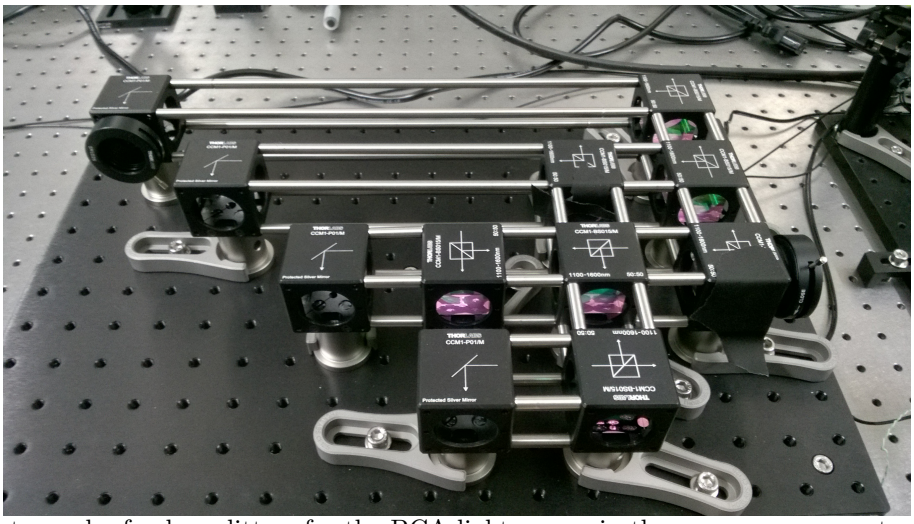

Figure 5: Photograph of cube splitters for the BCA light source in the same arrangement as in Figure 3.

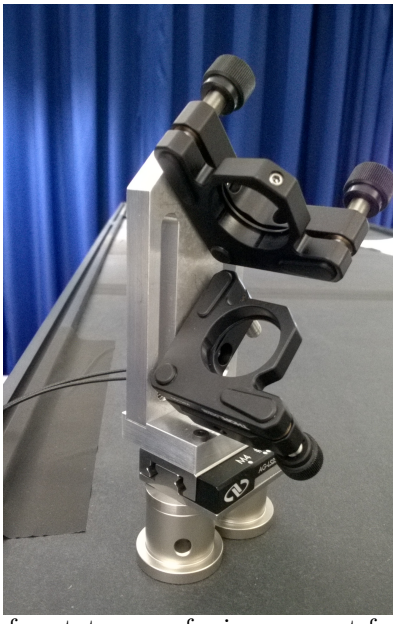

Figure 6: Photograph of prototype roof mirror mount for the BCA light source.

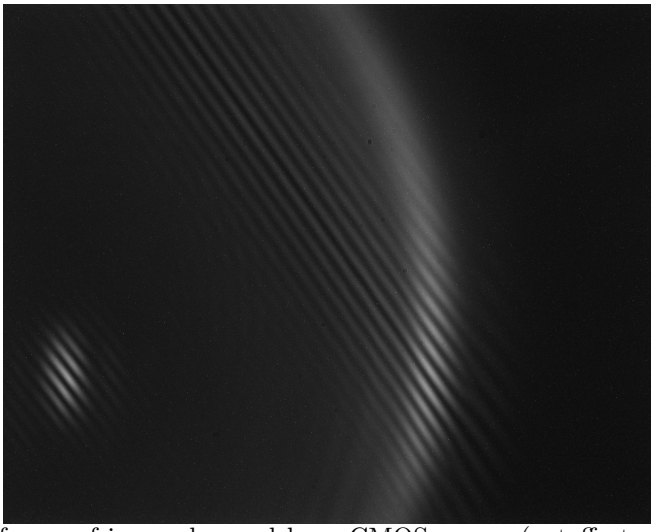

Figure 7: White light interference fringes observed by a CMOS sensor (cutoff at approximately 900nm). The intensity is greatest at the edge of the beam due to Fresnel diffraction. The beam on the left is a laser. The white light contrast is approximately 0.6.

### 3.3 Tilt and shear detection

#### 3.3.1 Concept

We will employ a Shack-Hartmann sensor to find the tilt and shear of a starlight beam in a single measurement - this appears to be a novel application of this well-known device. A Shack-Hartmann sensor consists of an array of microlenses with a camera sensor placed at their focal plane. A collimated beam at the input produces an array of spots at the sensor. If the input beam is tilted, the spots all move in the transverse direction by an amount proportional to the amount of tilt. Shear, on the other hand, is measured by reducing the Shack-Hartmann image to an array where each pixel has the dimensions of one microlens. Each pixel takes the value of the flux through its corresponding microlens. The movement of the centroid of this reduced image is recorded as shear. By recording both the tilt and shear at one plane, we fully characterise the alignment of the beam, yielding a compact detector that suffers fewer systematics than a conventional two-sensor arrangement.

#### 3.3.2 Laboratory Prototyping

We assembled a device from commercially available parts, summarised in Table 1. Our initial prototyping goals were to assess measurement sensitivity at low light levels and to quantify drifts due to ambient temperature changes. Several other behaviours were investigated, including detection linearity and the impact of non-flat wavefronts. The test light source was a 3mm-diameter collimated beam generated from a light emitting diode of centre wavelength 625nm.

Table 1: Properties of Shack-Hartmann sensor for prototyping.

| | |
|---|---|
| Microlens focal length | 18.6mm |
| Microlens pitch | 300$\mu$m |
| Microlens shape | Square, contiguous |
| Sensor type | CMOS |
| Sensor pixel size | 5.3$\mu$m $\times$ 5.3$\mu$m |
| Sensor dimensions | 6.8mm $\times$ 5.4mm |

Measurement sensitivity at low light levels is important since we seek to reduce observing time lost when recalibrating UTLIS with starlight. As a minimum requirement, we aim to use calibration stars brighter than $m_H = 1.5$ since there is a more than 50% probability of finding at least one such star within 10 degrees of any location in the sky. The slewing penalty would be a few tens of seconds a few times per hour. The sensitivity of the Shack-Hartmann sensor is ultimately limited by the accuracy of finding spot centroids. As the number of photons incident on the detector decreases, the photon shot noise increases and the signal level may be comparable to the sensor read noise. These sources of noise pull the measured centroid away from its true location. We estimated the detection sensitivity by keeping the beam stationary on the sensor and capturing a large sample of images. The tilt and shear between each image and a reference was computed, and this procedure was repeated over a range of irradiances. Figure 8 depicts the tilt and shear measurement accuracy as a function of the number of photons per unit area during a single exposure - this choice of units allows direct comparison with beam diameters at MROI. For light from a magnitude 1.5 star, the sensitivity is 0.23 arcseconds in tilt and 1.7$\mu$m in shear. One must treat these numbers carefully since measurement sensitivity not only depends on the number of photons arriving at the detector but also on the number of filled microlenses that contribute centroids, both for tilt averaging and for sampling the pupil. In prototyping, typically 10 $\times$ 10 microlenses were filled. Fewer microlenses may be filled in practice at MROI.

To address the second prototyping goal, we quantified the drift of tilt and shear measurements attributed to the Shack-Hartmann sensor in response to ambient temperature drifts. The inner BCA at MROI will be stabilised to $0.1^oC$, whereas overnight temperatures in our laboratory typically drop by 2K overnight; it was simple to correlate drifts of tilt and shear measurements with the change in ambient temperature. Upper limits

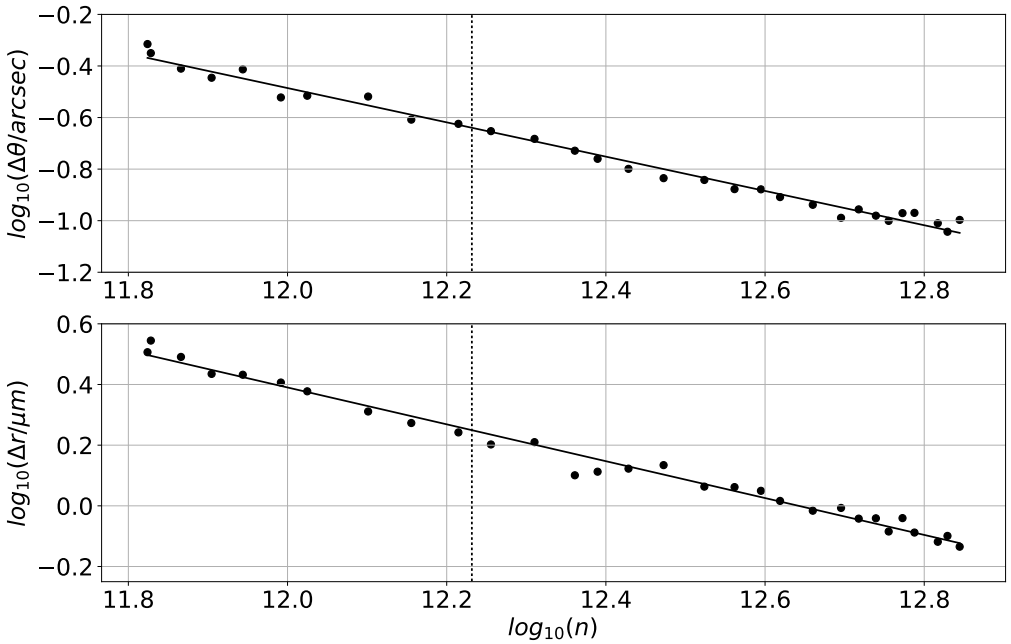


Figure 8: Tilt and shear measurement sensitivity as a function of number of incident photons for the prototype detector. $\Delta\theta$ and $\Delta r$ correspond to tilt and shear sensitivities, respectively. n refers to the number of photons per metre squared recorded by the camera during an exposure time. The dotted line marks the photon density incident on a tilt and shear detector at MROI for starlight of magnitude 1.5 that has been compressed by a factor of 2.

on two-axis drift in tilt and shear measurements were 0.5 arcsec per 0.1K and 5$\mu$m per 0.1K, respectively, at a beam diameter of approximately 3mm. Although these drifts are not excessively large, it would be helpful to pinpoint and mitigate their cause in future.

Shear detection linearity was determined by imparting a pure shear misalignment. The camera was mounted on a micrometer-actuated slide with resolution of 10$\mu$m. Two axis shear was recorded by the Shack-Hartmann sensor as a function of the movement shown by the micrometer. Figure 9 proves the linearity of the shear measurement over a range of 0.5mm.

Tilt detection linearity was determined by steering the beam with a Newport Agilis mirror mount in sub-arcsecond increments. This manifested as both a tilt and a shear on the detector. We utilised the shear as an independent method of measuring tilt since the distance between the mirror mount and Shack-Hartmann sensor was known. Figure 10 illustrates the linearity of tilt measurements. A linear response was recorded for the small tilts that we might expect to measure at MROI. The recorded value is systematically larger than the applied value due to the following reasoning.

Imagine a spherical wavefront incident on the microlens array. If the pupil becomes sheared, then a tilt is recorded that is proportional to both the radius of curvature of the wavefront and the amount of apparent shear. The origin of this tilt can be explained with reference to Figure 11, which shows the difference between two parabolic wavefronts.

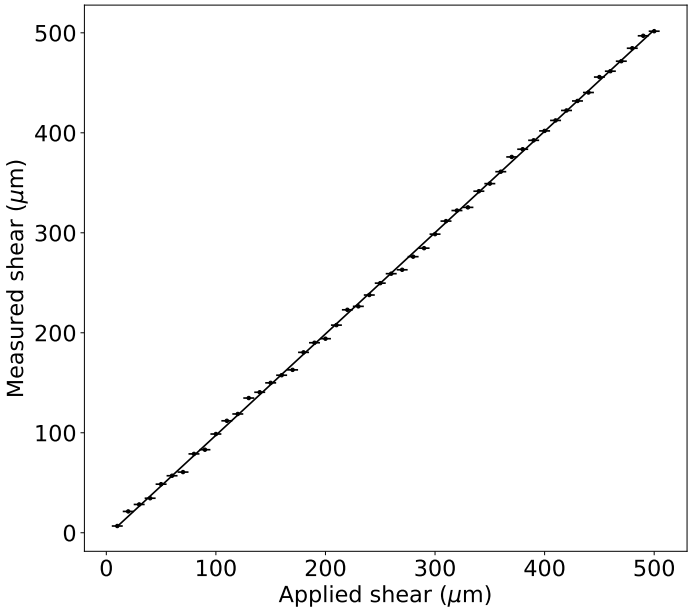


Figure 9: Linearity of shear detection measured by applying an independently verified shear.

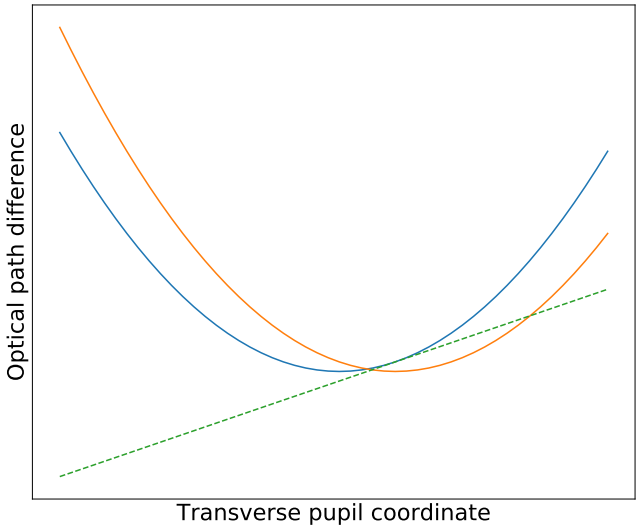


Figure 11: Demonstration of additional tilt caused by shearing curved wavefronts. The solid lines denote a curved wavefront has been sheared. The dashed line shows the difference between them, as would be computed by a Shack-Hartmann tilt detector. A slope in optical path difference corresponds to a beam tilt, and so an extra tilt component would be recorded by the Shack-Hartmann sensor.

Fortunately, with a Shack-Hartmann sensor we can directly measure the radius of curvature by computing the spacing between the focussed spots at the detector plane. For a perfectly spherical wavefront, this spacing

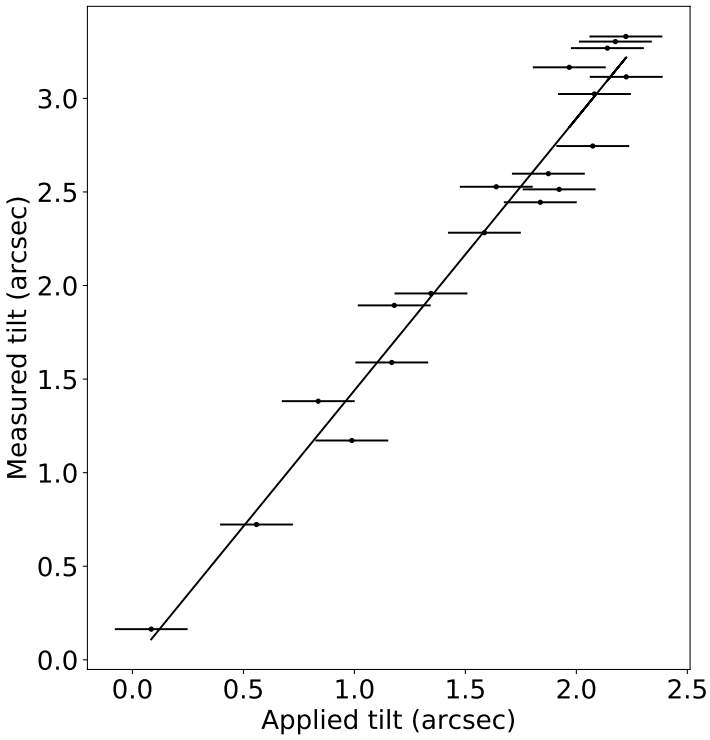


Figure 10: Linearity of tilt detection measured by applying an independently verified tilt.

is identical between all adjacent spots. In reality there will be systematic perturbations to the wavefront due to non-uniformities in optical surfaces and diffraction over long distances. In principle, one could subtract this extra term using knowledge of the wavefront shape.

### 3.3.3 Simulation

Astronomical seeing is an important effect that the laboratory prototype cannot test. There are two detrimental effects of a turbulent atmosphere. The first is that each subaperture of the telescope pupil is imparted with a differing phase perturbation. Each subaperture of the Shack-Hartmann array therefore receives an additional random component of tilt. The second effect is a variation of the pupil intensity distribution due to near field diffraction of a corrugated wavefront changing randomly in time; this disturbs the measured centroid of the input pupil for the tilt and shear detector.

Both of these effects can be mitigated by averaging over many exposures, but we seek to quantify any residual perturbations to tilt and shear measurements. We have developed a simulation of the intensity distribution arriving at the tilt and shear detector based upon diffraction code used in Horton et al.[6] We generated a Kolgmogarov phase screen and masked it with the UT pupil, including a central obscuration and a trio of spider vanes. The resulting complex amplitude distribution is propagated over a distance of approximately 350m by Fresnel diffraction,[7] including several stages of beam compression. Each loop of the simulation corresponds to a characteristic timescale defined by $t_0 = 0.314 r_0 / v_{avg}$, where $r_0$ is the Fried parameter and $v_{avg}$ is the wind speed averaged across turbulent layers. We generate an independent atmospheric phase screen for each $t_0$. For $v_{avg} = 10 ms^{-1}$ and $r_0 = 40 cm$, $t_0 = 12.7 ms$. Figure 12 shows the pupil intensity distribution after different propagation lengths for cases of a single subexposure with no turbulence, a single subexposure including Kolmogarov turbulence and finally an average of 100 subexposures in the presence of Kolmogarov turbulence.

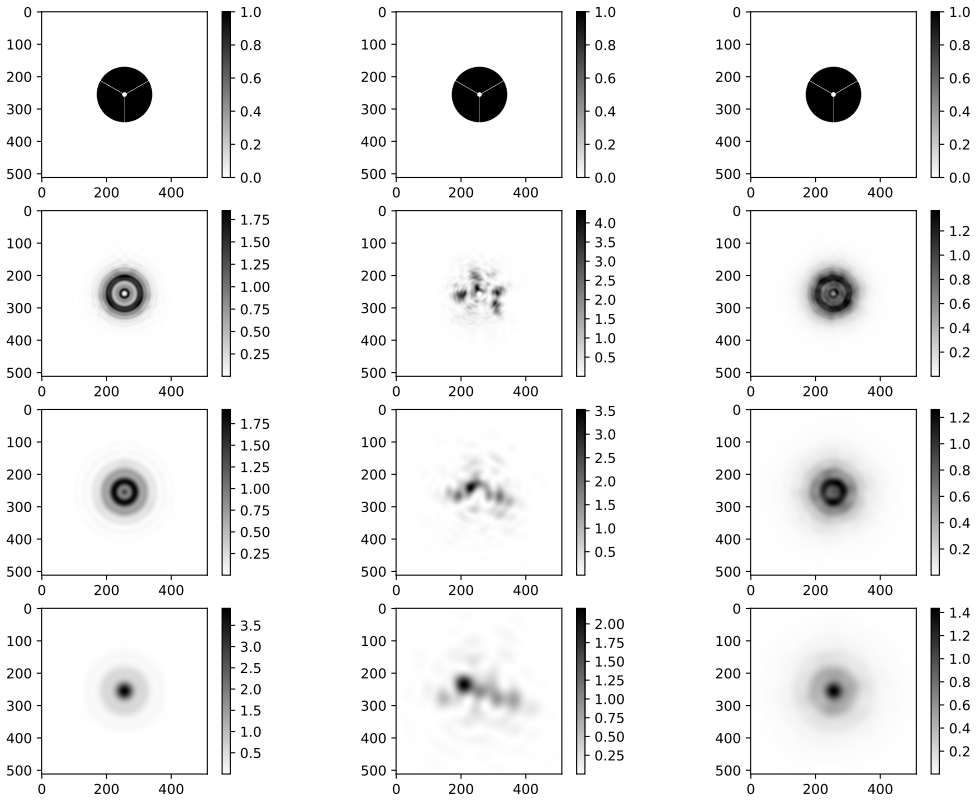

Figure 12: Simulated pupil intensities at MROI after propagation for cases of no turbulence (left column), Kolmogarov turbulence in a single exposure (centre column) and Kolmogarov turbulence averaged over 100 exposures (right column). The pupils are sampled at the unit telescope (first row), after propagation by 340m in the beam relay system (second row), after further propagation by 10m in the BCA (third row) and after final propagation by 0.3m to the alignment camera (fourth row). Pixel units are scaled to the nominal beam diameter at each point along the beam path.

The input pupil for the detector was passed through a phase screen representing the microlens array in order to simulate the Shack-Hartmann sensor. Figure 13 highlights the difference between a single exposure lasting $t_0$ and an average of 100 exposures of individual duration $t_0$.

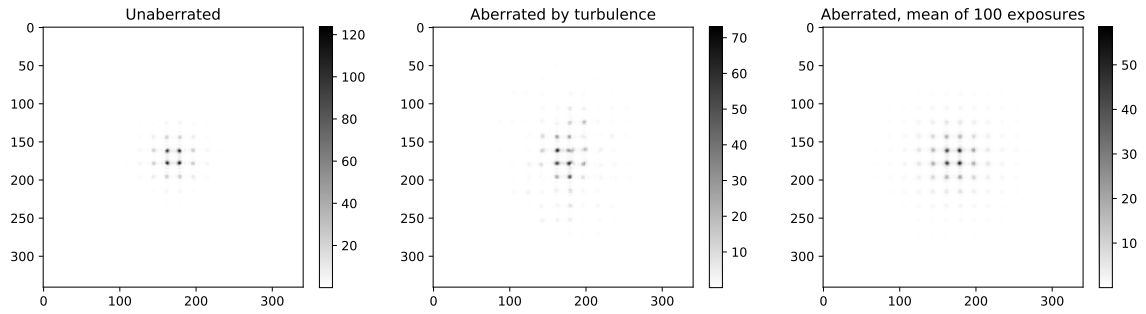


Figure 13: Comparison of Shack-Hartmann images with exposures lasting $t_0$ for the input pupils displayed in Figure 12.

The Shack-Hartmann sensor to be deployed at MROI will use an InGaAs CCD that is sensitive to short-wave infrared wavelengths. These sensors typically exhibit greater read noise and dark current than their visible counterparts, therefore we generated a noise profile using manufacturer specifications for read noise and the number of dark electrons per second of exposure. We must also consider photon shot noise, which may impact upon centroiding for dim starlight.

To assess the impact of each noise contribution, we generated a sample of 200 images of a stationary beam under different sets of noise conditions. The tilt and shear of each image was computed with respect to a reference. Then the standard deviation of the sample of tilts and shears was recorded as the measurement sensitivity. The exposure time was 100ms while the spot size was defined for a wavelength of 1.6$\mu$m. The results are given in Table 2. Note that these values have been calculated for a beam compressed by a factor of 6. This amplifies apparent tilt while reducing apparent shear. Hence when all noise sources are present, the sensitivities are likely to be 0.40 arcseconds in tilt and 29 $\mu m$ in shear at the BCA beam diameter of 13mm. Interestingly, the combination of photon noise, camera noise and turbulence generates more scatter than the root square sum of their individual contributions. Future investigations may shed light on why this might be the case.

Table 2: Simulated tilt and shear sensitivities in the presence of realistic noise sources for light from a Magnitude 4 star, recorded with subexposures of 100ms and averaged over 5s.

| Conditions | Tilt sensitivity (arcsec) | Shear sensitivity ($\mu$m) |
|---|---|---|
| Photon noise only | 0.13 | 0.20 |
| Camera noise only | 0.92 | 0.21 |
| Turbulence noise only | 0.74 | 4.34 |
| Camera, turbulence and photon noise | 2.41 | 4.84 |

### 3.3.4 Design

Our findings from the prototyping phase have led us towards the design of the tilt and shear detector visualised in Figure 14. Roughly 2% of the starlight beam will be picked off using a parallel window with a R=1% antireflection coating on both surfaces. The light is then fed into a 6x reflective beam compressor that reduces the 13mm diameter starlight beam to a size smaller than readily available InGaAs sensors. To mitigate the elongation of Shack-Hartmann spots at bluer wavelengths by atmospheric refraction, we employ a longpass filter with a cutoff at 1.1$\mu$m. The upper limit of the bandpass is determined by the InGaAs sensor, which cuts off at 1.7$\mu$m. An anti-reflection coated microlens array is attached by C-mount. The camera consumes up to 2.5W, so it will be housed in an insulated box that is connected to a heat vent on the ceiling by a flexible chimney.

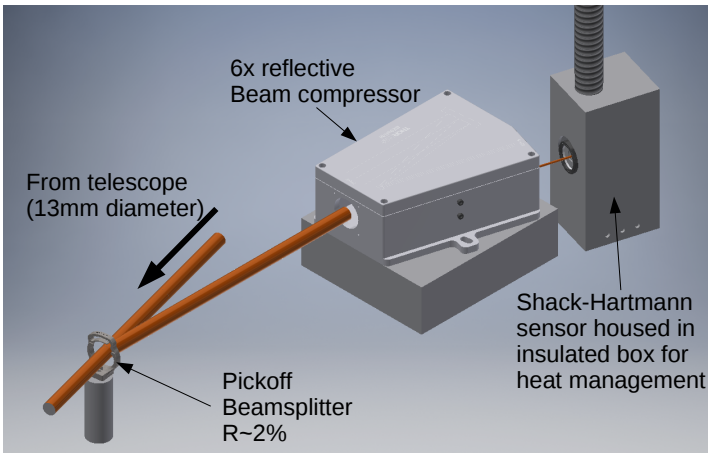


Figure 14: Tilt and shear detection hardware comprising of a pickoff beam splitter, beam compressor and Shack-Hartmann sensor.

## 4. FUTURE DEVELOPMENT

An intermediate version of the tilt and shear detector will be tested on sky at MROI in late 2018 for an important commissioning milestone. Final versions of all components of the AAS are expected to be installed on site in 2019.

## ACKNOWLEDGMENTS

This material is based on research sponsored by Air Force Research Laboratory (AFRL) under agreement number FA9453-15-2-0086. The U.S. Government is authorized to reproduce and distribute reprints for Governmental purposes notwithstanding any copyright notation thereon. The views and conclusions contained herein are those of the authors and should not be interpreted as necessarily representing the official policies or endorsements, either expressed or implied, of Air Force Research Laboratory (AFRL) and or the U.S. Government. The work has also been partially supported by a Science & Technology Facilities Council studentship.

## REFERENCES

[1] Buscher, D. F., Creech-Eakman, M., Farris, A., Haniff, C. A., and Young, J. S., "The conceptual design of the Magdalena Ridge Observatory Interferometer," *J. Astron Instrum* **2** (2013).

[2] Shtromberg, A. V., Jurgenson, C. A., McCord, K. M., Olivares, A. M., Bloemhard, H. N., Santoro, F. G., Buscher, D. F., Haniff, C. A., Young, J. S., Torres, N. C., and Farris, A. R., "Magdalena Ridge Observatory Interferometer automated alignment system," *Proc. SPIE*, 773411 (2010).

[3] Young, J., Buscher, D., Fisher, M., Haniff, C., Rea, A., Seneta, E. B., Sun, X., Wilson, D., Farris, A., Olivares, A., and Selina, R., "The MROI fast tip-tilt correction and target acquisition system," *Proc. SPIE*, 844515 (2012).

[4] Buscher, D. F., [*Practical Optical Interferometry*], Cambridge University Press, Cambridge (2015).

[5] Hobson, M. P. and Baldwin, J. E., "Markov-chain Monte Carlo approach to the design of multilayer thin-film optical coatings," *Applied Optics* **43**, 2651–2660 (2004).

[6] Horton, A. J., Buscher, D. F., and Haniff, C. A., "Diffraction losses in ground based optical interferometers," *MNRAS* **327**, 217–226 (2001).

[7] Goodman, J. W., [*Introduction to Fourier Optics*], McGraw-Hill, New York (1996 (second edition)).